HEAT TRANSFER TO A MOVING WIRE IMMERSED IN A GAS FLUIDIZED BED FURNACE

by

Shanta Mazumder

Bachelor of Mechanical Engineering

Ryerson University, 2014

A MRP

presented to Ryerson University

in partial fulfillment of the

requirements for the degree of

Master of Engineering

in the program of

Mechanical Engineering

Toronto, Ontario, Canada, 2016

Author's Declaration

I hereby declare that I am the sole author of this MRP. This is a true copy of the MRP, including any required final revisions, as accepted by my examiner.

I authorize Ryerson University to lend this MRP to other institutions or individuals for the purpose of scholarly research.

I further authorize Ryerson University to reproduce this MRP by photocopying or by other means, in total or in part, at the request of other institutions or individuals for the purpose of scholarly research.

I understand that my MRP may be made electronically available to the public.

Abstract

Heat Transfer to a Moving Wire Immersed in a Gas Fluidized Bed Furnace

Shanta Mazumder, Master of Engineering, Mechanical and Industrial Engineering, 2016 Ryerson University

The gasified fluidized bed has been looked at as a safer replacement for heat treatment of carbon steel wire traditionally heat treated using molten lead baths. Most of the research has been conducted on heat transfer to larger diameter boiler tubes immersed in gas fluidized beds used by the power generation industry. However, there has been a lack of research on small diameter cylinders and longitudinally moving wire in heat treating systems. In 2015, Tannas developed a correlation that confirmed that the correlation previously developed for static wire under-predicts the heat transfer rate at higher wire speeds. In addition, this earlier correlation did not account for varying fluidization rates and only assumed that Nu was independent of fluidization rate for $U_g/U_{mf} > 2.5$. So, the work reported here is intended to develop a new correlation that accounts for both wire motion and fluidizing rate in fluidized bed.

Acknowledgements

I would like to thank my supervisor Dr. Jacob Friedman and Antonio Tannas for all the support, guidance and giving me this opportunity to explore and learn.

I would also like to thank my brother and my parents for their endless support. Without it, I wouldn’t be here.

Finally, thank you to Ryerson University, Mechanical and Industrial Engineering department, the Natural Sciences and Engineering Research Council of Canada and Wirekorner Gmbh for their generous support.

Table of Contents

List of Tables

List of Figures

Nomenclature

μ_g	Viscosity of the gas (k_g/sm)
$\emptyset_s$	Particle Sphericity
ρ_b	Bulk Density of bed (k_g/m^3)
ρ_g	Gas Density (k_g/m^3)
ρ_s	Particle Density (k_g/m^3)
ρ_w	Wire Density (k_g/m^3)
τ	Particle or cluster residence time at the surface (s)
θ (x)	Temperature difference between the bed and wire temperatures = $T(x) - T_\infty$ (℃)
θ_{in}	Temperature difference between the bed and wire inlet temperatures = $T_{in} - T_\infty$ (℃)
ϵ	Bed Voidage
A_b	Effective bed area (m^2)
A_c	Wire cross sectional area (m^2)
Ar	Archimedes number $= \frac{g\rho_g(\rho_p - \rho_g)d_p^3}{\mu_g^2}$
$C_{p,g}$	Specific Heat Capacity of the gas (J/k_gK)
$C_{p,s}$	Specific Heat Capacity of the particles (J/k_gK)
$C_{p,w}$	Specific Heat Capacity of the wire (J/k_gK)
D_b	Fluidized bed diameter (m)
d_p	Mean particles diameter (m)

D_{sv}	Diameter of a sphere having the same surface/volume ratio as the particle (m)
G	Fluidizing mass flow rate (k_g/s)
G_{mf}	Minimum fluidizing mass flow rate (k_g/s)
H	Bed Height (m)
h	Heat Transfer coefficient (W/m^2K)
k_c	Thermal conductivity of the cluster (W/mK)
k_g	Thermal conductivity of the gas (W/mK)
k_w	Thermal conductivity of the wire (W/mK)
m	Mass of the particles in the bed (k_g)
Δp	Pressure drop across the bed (Pa)
$\bar{p}$	Average Absolute Pressure in the bed (Pa)
P	Perimeter of immersed cylinder (m)
p_{in}	Absolute Pressure at bed inlet (Pa)
Q_x	Heat Flux at current location (W/m^2)
T(x)	Temperature at current location (℃)
$T_{in_{measured}}$	Inlet Temperature as measure by thermocouple (℃)
T_∞	Outlet Temperature as measure by thermocouple (℃)
U	Current Fluidizing rate (m/s)

1 Introduction

Fluidization is not a new phenomenon. The widespread commercial use of this technology began in 1940 with the construction of the first fluid bed catalytic cracker (FCC) [2]. In this process a bed of solid particles are suspended by an upward flow of gas or liquid and behave as if they are in a fluid-like state. This technology is divided into two parts according to its application in industrial processes: physical and chemical. Some of the physical applications include heat treatment of wire, plastic coating of surfaces, drying, food freezing, and some chemical applications including oil cracking, coal combustion, coal gasification etc [2]. Figure 1 below shows various categories of applications currently found in industrial processes. Another well known area where this technology is being used is nuclear engineering. Its application is seen in uranium extraction, nuclear fuel fabrication, reprocessing of fuel and waste disposal [2].

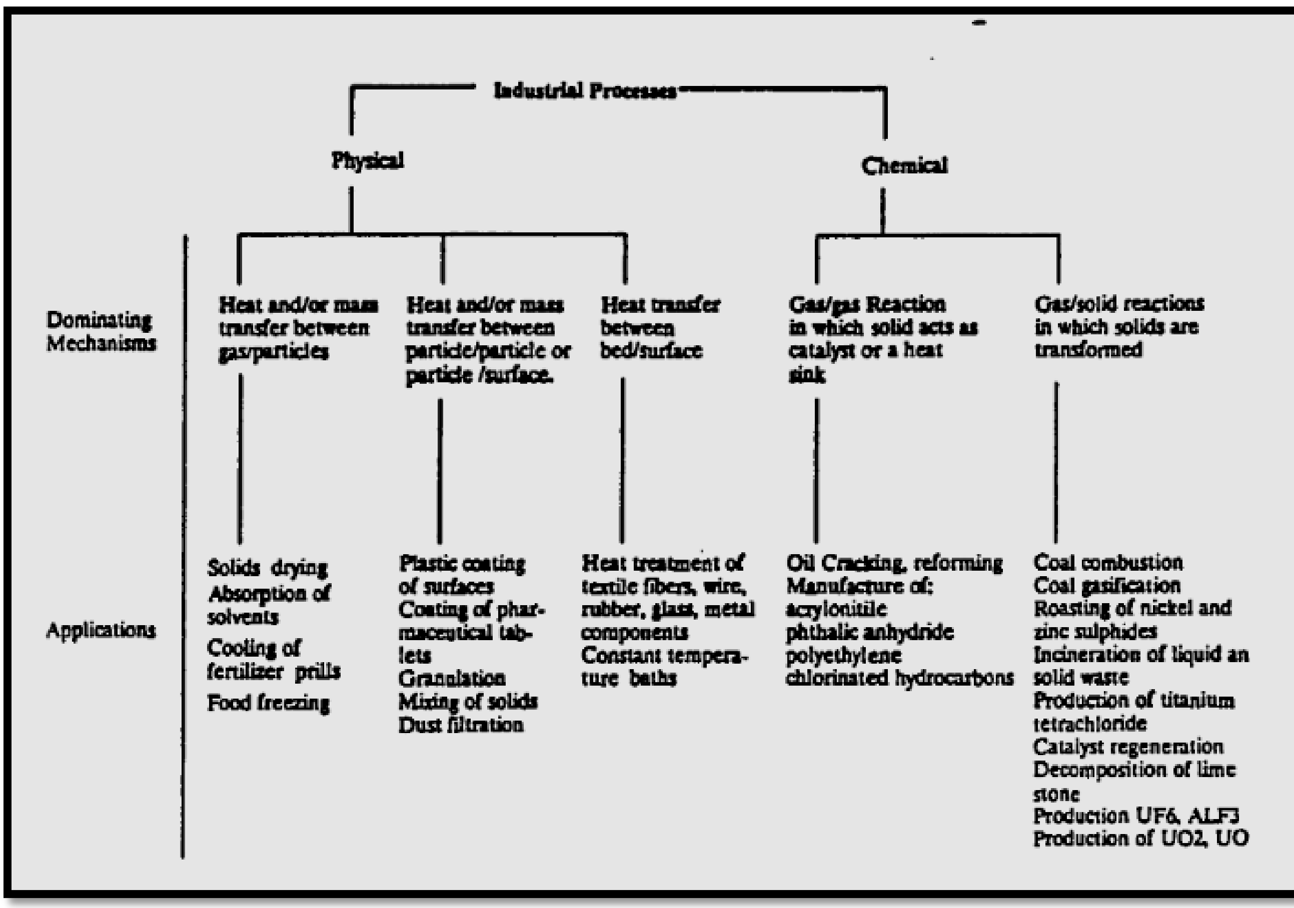

Figure 1: Classification of fluid bed applications according to predominating mechanisms [2].

It is mentioned above that heat treatment of wire is one of the many applications where fluidized bed technology is being used. Heat treatment is applied to steel wire (low carbon and high carbon) to reduce work hardening that is caused from drawing the wire through dies and to increase strength and ductility. At present, it is still a very common practice to use a molten lead bath in the heat treatment process. A schematic of the wire drawing and heat treatment process using a molten lead bath is shown in Figure 2. Molten lead baths are known to provide high heat transfer rates. But the lead is very toxic and harmful for both the worker and the environment [1]. The fluidized bed furnace, on the other hand, is capable of providing relatively high heat transfer rates and good temperature uniformity without the health risk to the worker and environmental hazards. However, due to inadequate knowledge of heat transfer rates, it is still not a well adopted technology for high carbon steel wire in industry. And heat treatment of high carbon steel is a more demanding process than for low carbon steel, requiring precise control of temperature and heating/cooling rates.

In the past there have been extensive studies on heat transfer to boiler tubes ranging from 25-50 mm in diameter by the power generation industry, but the correlations developed show contradictory results when applied to smaller diameters [1]. In recent years, several studies have looked into heat transfer to small diameter cylinders, but only in static mode. Hence, the effect of longitudinal motion on heat transfer rate is not yet known. In 2008, a study conducted by Masoumifard et al. [3] showed the influence of axial position, particle diameter and superficial gas velocity on the heat transfer coefficients from an 8 mm tube immersed in the fluidized bed. A correlation was developed based on a cluster renewal method that showed that heat transfer rate was highly dependent on the contact time (τ) between the immersed surface and the particles [3]. But any motion of the immersed surface can alter this contact time (τ).

With this intention, the first laboratory scale wire movement system that passes a wire longitudinally through a fluidized bed furnace was developed by Antonio Tannas, at Ryerson University's Fluidized Bed Heat Transfer Laboratory. His work [1] led to development of a correlation that considers the effect of wire movement and different particle sizes. However, it assumes that the heat transfer coefficient (h) is not affected by fluidizing rates past $U_g \geq 2.5 \times U_{mf}$.

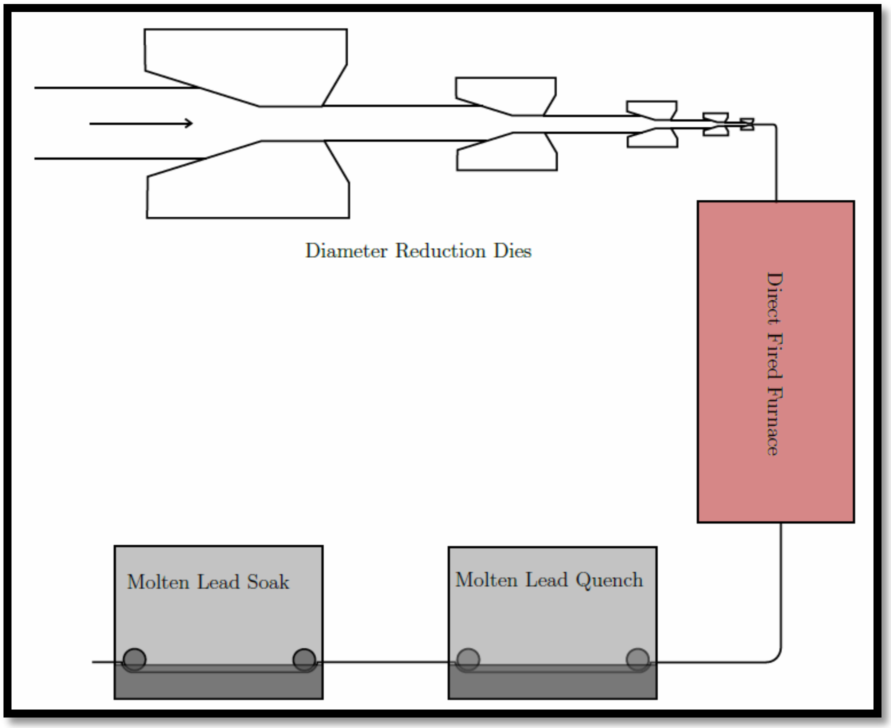

Figure 2: Wire drawing and heat treatment process [1].

Therefore, the main purpose of this report is to:

1. Improve the understanding of fluidized bed technology and identify the parameters affecting heat transfer in the context of wire heat treatment.
2. Conduct further experiments to develop a simple correlation that can be used for the design of wire heat treating systems that accounts for both longitudinal motion and varying fluidizing rate.

1.1 Literature Review

There have been numerous attempts to determine the heat transfer rate to immersed surfaces in fluidized beds in the past, mostly motivated by the power generation industry. The majority of these works were focused on larger diameter boiler tubes ranging from 25 mm to 50 mm used in coal combustion boilers [1]. In recent years, there have been some significant studies on small diameter cylinders ranging from 1 mm to 9.5 mm, were conducted by Friedman et al. [4], and Masoumifard et al. [3,5] in 2006, 2008 and 2010 respectively. However, none of these studies involved longitudinal movement of the cylinders.

In 2006, Friedman et al. [4] conducted a study on heat transfer to stationary small diameter cylinders ranging from 1.3-9.5 mm diameter. Results showed that correlations developed for larger diameter tubes over-predict the heat transfer from small diameter tubes [4]. A nearly constant heat transfer rate was also observed after $2.5 \times \frac{G}{G_{mf}}$ (G is gas fluidizing mass flux) [4]. Their developed correlation is given below:

$$\mathrm{Nu_{mean}} = \left[1.35\ \mathrm{Ar}^{0.15}\,\frac{d_t}{d_p}\right] \tag{1}$$

where,

$$\mathrm{Ar} = \frac{g\rho_g(\rho_p - \rho_g)d_p^3}{\mu_g^2} \tag{2}$$

This correlation is dependent on Archimedes number and the ratio of tube diameter to the diameter of the sand particles [4]. It was also proven suitable for engineering application and able to predict heat transfer rates for smaller diameter cylinders [4].

In 2008, Masoumifard et al. [3] conducted a study on heat transfer from an 8 mm diameter cylinder immersed in a fluidized bed. The study focused on the influence of the axial position, particle diameter and superficial gas velocity on the heat transfer coefficient. They found that heat transfer is independent of axial position and heat transfer is inversely proportional to the particle diameter [3]. Their developed correlation was based on the cluster renewal method and was successful at predicting heat transfer which highly depends on the duration of the contact time (τ) between the immersed cylinder and the particle clusters [3]. According to Masoumifard et al. "High heat transfer coefficient is achieved with shorter residence time or clusters with higher solid holdups" [3].

In 2010, another study on the same model was conducted to predict the maximum heat transfer coefficient and superficial air velocity [5]. They found that the maximum heat transfer rate would occur when the contact time (τ) is equal to the time it takes for the heat to completely diffuse inside the cluster (t_o) [5]. Their developed complex correlation model predicted optimal superficial air velocity and heat transfer within $\pm 20\%$ of uncertainty [5]. But the complex nature of this model makes it difficult to apply in small engineering applications.

In 2015, a study on predicting the heat transfer coefficient for moving wire through a fluidized bed was conducted by Tannas [1]. He developed a continuous wire drawing mechanism that passes wire at constant velocity through a fluidized bed. Using collected data for parameters such as inlet temperature, outlet temperature, bed temperature, wire speed etc. he was able to develop the following correlation:

$$\mathrm{Nu}_{\mathrm{mean,moving}} = \left[1.35\ \mathrm{Ar}^{0.15}\frac{\mathrm{D_t}}{\mathrm{d_p}}\right] \times [1 + 0.02(\frac{\mathrm{u_w}}{\mathrm{U_{mf}}})^{0.5}] \tag{3}$$

$$\mathrm{U_{mf}} = \frac{\mu_g}{\rho_g \mathrm{d_p}}\ [(1135.7 + 0.0408\ \mathrm{Ar})^{\frac{1}{2}} - 33.7] \tag{4}$$

This correlation showed that the movement of the wire does affect the overall heat transfer coefficient [1]. It is valid for fluidizing rate, $\frac{u_g}{U_{mf}} > 2.5$ and assumes that the heat transfer coefficient (h) is independent of $\frac{u_g}{U_{mf}}$ as long as $\frac{u_g}{U_{mf}} > 2.5$ [1]. All the experimental data predicted using this correlation was within $\pm 15\%$ margin of error [1].

While the above correlation gives better insight into heat transfer to a moving wire immersed in a fluidizing bed, more experiments are required to expand the data set and develop a modified simple correlation that is also dependent on fluidizing rates $\frac{u_g}{U_{mf}}$, as it was apparent that the assumption of independence of Nu from fluidizing rate was weak, especially for fluidizing rates $\frac{u_g}{U_{mf}} < 2.5$.

2 Theoretical Considerations

2.1 Gas Fluidization

The primary components of a gas fluidized bed are a vessel or container filled with granular solid particles, a blower for providing pressurized gas and a porous distributor to support the solid particles and distribute the pressurized gas [1]. Components can be assembled into many forms and some of the common forms of fluidized bed are shown in Figure 3 below. The main characteristics of gas fluidized beds are that they provide good solids mixing through rapid motion of particles; good temperature uniformity; there is also a large surface area of solid particles available for heat exchange with the fluidizing gas [6].

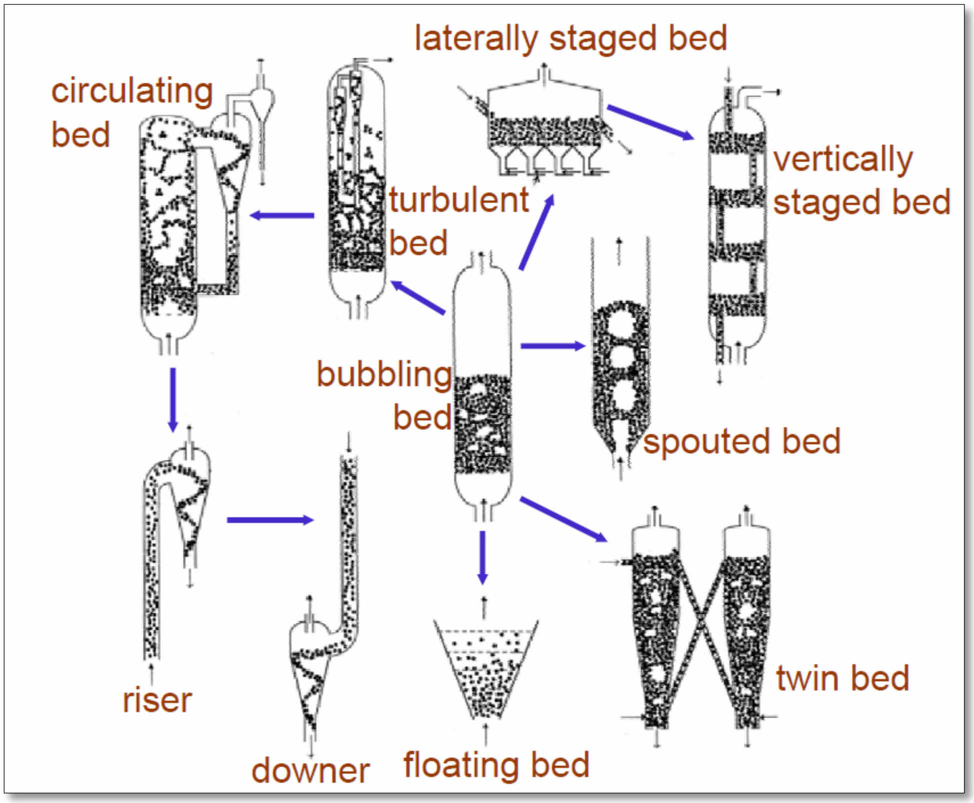

Figure 3: Various forms of fluidized bed [7].

2.2 States of Fluidization

Fluidization is a continuous process. There are a number of stages that take the static packed bed to the fully fluidized state. At first, when the fluid flow is initialized, the bed of particles starts vibrating [1]. No expansion of the bed height is seen at this stage as the fluid passes through solids with greater resistance [1]. Gradually, particles rearrange themselves and offer less resistance [1]. Then, when velocity becomes high enough and pressure drop equals the bed weight, packing and interlocking forces break up and particles starts to fluidize [1]. At this point the drag force on the particles is equal to the particle weight per bed area and this point is known as incipient fluidization [1].

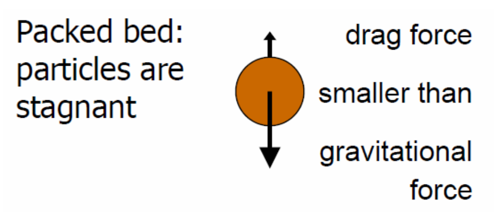

Figure 4: Illustration of first stage of fluidization [7].

Further increasing the fluid velocity leads to bed expansion and bubble formation [1]. Pressure drop in this region stays constant [1]. And after some time, bubbles start to coalesce to form larger bubbles [1]. This causes the local density of the packing to increase and initiate particle circulation where particle circulation is directly proportional to the heat transfer rate [1]. Finally, when the fluid velocity increases even further, the drag force on the particles increases and carries the particles out of the bed [1]. Pressure drop also increases at this state [1]. Figure 5 below shows various states of fluidization:

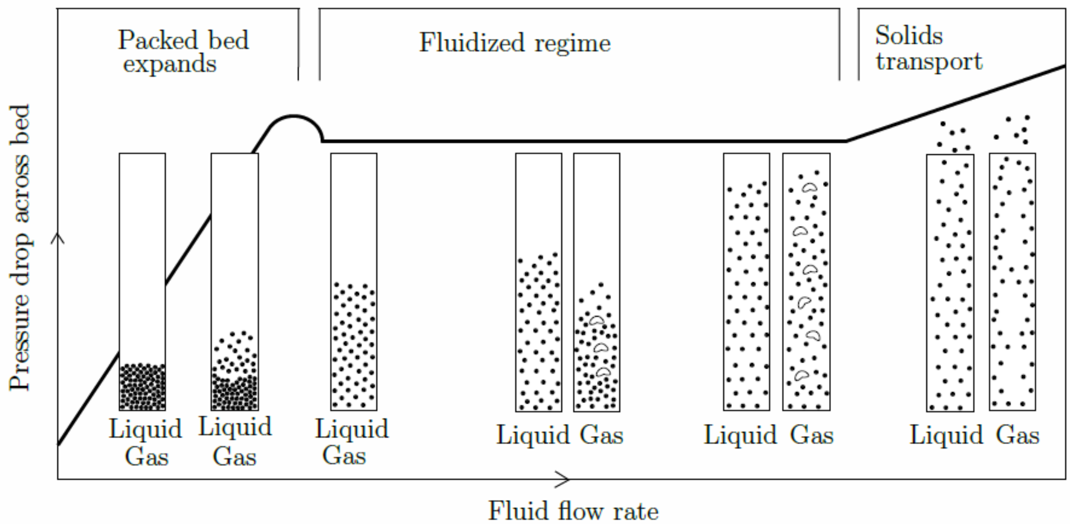

Figure 5: Regimes of fluidization [1].

2.3 Classification of Particles

Particles play a crucial role in fluidization. Geldart [2] categorized four groups of particles based on density and size. Figure 6 illustrates the different groups on a graph according to density and diameter.

Group A: This group of particles are most used commercially and have been extensively studied over the past [2]. They are also known as 'aeratable' particles [2]. Mean particle diameter, d_p is < 30 μm and/or low particle density is <~1.4 g/cm^3 [2]. This group exhibit easy and smooth fluidization at low gas velocity and at higher gas velocity, minimum bubbling velocity is seen to be always greater than the minimum fluidization velocity [2].

Group B: This group is known as 'sandlike' particles. Typically, mean particle diameter is between 150 μm and 500 μm and density is between 1.4 to 4 g/cm^3 [2]. Due to low inter-locking forces, minimal bed expansion is seen [2]. Once the minimum fluidization state is reached excess bubble formation is seen [2]. Examples of this group of particles are glass beads and coarse sand [2]. The current study considers particles belonging to group B.

Group C: This group of particles are 'cohesive' or very fine powders. Typically mean particle diameter is less than 30 μm [2]. They are also extremely difficult to fluidize [1]. Examples of this group are talc, flour and starch [2].

Group D: Also known as 'spoutable'. These particles are very large and dense in nature [2]. They are also very difficult to fluidize. Examples include: roasting coffee beans, lead shot and roasting metal ores [2].

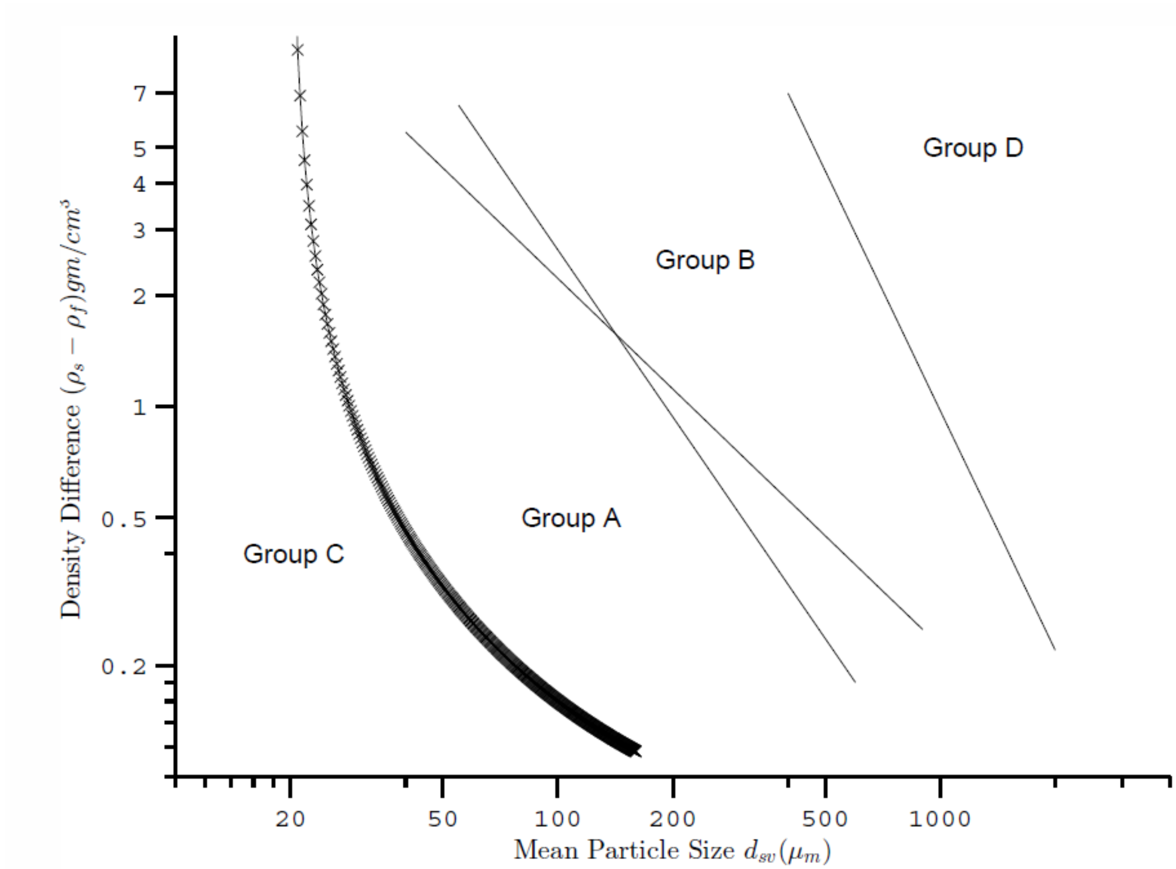

Figure 6: Geldart's classification of powders [1].

2.4 Pressure Drop through a Bed

Pressure drop through the bed can be calculated using Equation 5 below [1]:

$$\Delta p = (1-\varepsilon) g \rho_s H \tag{5}$$

where,

$\varepsilon \equiv$ (Volume of Bed -Volume of Particles)/Volume of Bed [1]

$$\varepsilon = 1 - \frac{\rho_b}{\rho_s} \tag{6}$$

ρ_b = Bulk Density of Bed (kg/m^3)

ρ_s = Density of Solid Particles (kg/m^3)

g = Acceleration due to gravity (9.81 m/s^2)

H = Height of Bed (m)

Since Equation 5 does not take fluid velocity into account, a commonly used equation known as the Ergun equation (Equation 7) is used to represent flow conditions inside a fluidized bed [1]. It can be used to determine pressure drop at any vertical point inside a fluidized bed [1]. This equation consists of two parts, first laminar and second turbulent [1].

$$\frac{\Delta p}{H} = \frac{p_{in}}{\bar{p}} \left[150 \frac{(1-\varepsilon)^2}{\varepsilon^3} \frac{\mu_g U}{{d_{sv}}^2} + 1.75 \frac{(1-\varepsilon)}{\varepsilon^3} \frac{\rho_g U^2}{d_{sv}} \right] \tag{7}$$

where,

$\frac{p_{in}}{\bar{p}}$ = Correction Factor for Compressibility

p_{in} = Absolute Pressure at Bed Inlet (Pa)

$\bar{p}$ = Average Absolute Pressure in the Bed (Pa)

μ_g = Gas Viscosity (k$_g$/ms)

U = Fluidizing Velocity (m/s)

d_{sv} = Diameter of a Sphere with the same Surface/Volume Ratio as the particle (m^2)

In case of laminar flow ($Re_p < 1$), the above equation becomes:

$$\frac{\Delta p}{H} = \frac{(1-\varepsilon)^2}{\varepsilon^3} \frac{K \mu_g U}{d_p{}^2} \qquad (8)$$

This Equation 8 is also known as Carman-Kozeny equation [1].

where,

$K = 180$ for $0.4 \leq \varepsilon \leq 0.5$ and $0.1 \leq Re_p \leq 1.0$

d_p= Mean Particle Diameter (m)

2.5 Minimum Fluidization Velocity

The fluidized bed reaches the minimum fluidization state when the drag force on the particle is equal to the weight of the particle.

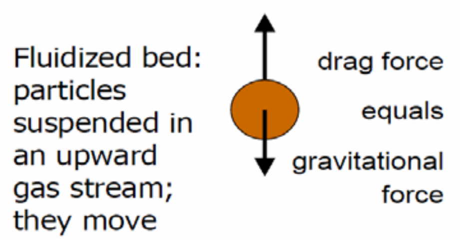

Figure 7: Illustration of minimum fluidization [7].

The Carman-Kozeny Equation 8 shows linear relationship between pressure drop and fluid velocity [1]. But at the point of incipient fluidization, this relationship is no longer valid and the velocity at this point is the Minimum Fluidization Velocity (U_{mf}) [1]. The minimum fluidization velocity can be defined using Equation 4 and it is only applicable for particles greater than 100μm of diameter [1].

2.6 Heat Transfer in a Fluidized Bed

The fluidized bed is capable of providing high heat transfer rates to immersed surfaces. The large surface area of solid particles results in rapid heat transfer between the fluid and solid particle inside a fluidized bed [1]. The fluidized bed heat capacity can be on the order of 10^6 J/m^3K and the heat transfer coefficient can range from 250-700 W/ m^2K [1]. The fluidized bed also offers a greater degree of solid mixing which results in a uniform temperature distribution throughout the bed.

Heat transfer in the fluidized bed takes place in three modes: 1) particle convection, 2) gas convection and 3) radiation. Particle convection takes place between a solid particle and a surface through a small volume of gas (referred to as a “gas lens” shown on Figure 8) [1].The other two modes of heat transfer are gas convection and radiation. The gas convection mode of heat transfer take place when a flow of gas passes over the surface and the radiation mode of heat transfer take place from the particles to the surface [1]. Flow conditions, properties of the particles and temperature are important parameters that affect the magnitude of heat transfer. The overall heat transfer rate is then calculated by adding all three modes of heat transfer.

The type of particle used in a fluidized bed also affects the heat transfer coefficient. Particles belonging to Group A (fine particles) exhibit a higher degree of particle convection through high particle circulation. This group of particles also shows a greater heat capacity than the gas [1]. Particles belonging to Group D (large, heavy particles) exhibit a high degree of gas convection due to low circulation of particles [1]. Particles belonging to group B and C show a mix of particle and gas convection as the main modes of heat transfer [1]. High gas velocities lead to a shorter residence time which allows the surface to have more contact between fresh particles [1]. However, an optimal state is reached where the heat transfer reaches a maximum. Further increasing gas velocity leads to a lower heat transfer rate [1].

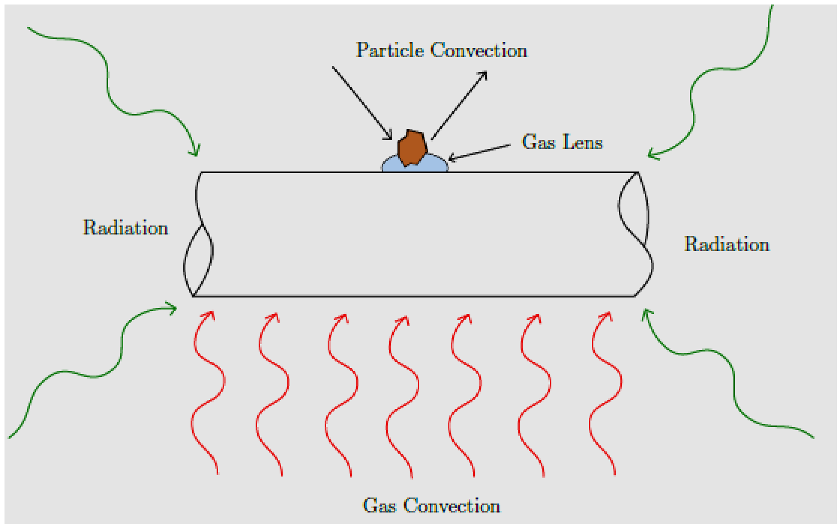

Figure 8: Modes of heat transfer in gas fluidized beds [1].

2.7 Effects of Wire Movement

Movement of wire can impact the residence time (τ) of particles and which can affect the heat transfer [1]. In the Figure 9, a highlighted red region is seen. The size of this red region reflects the contact time of wire with the fluidizing medium [1]. The shape of this region on the other hand represents the effect of wire speed and fluidization velocity [1]. At low fluidizing velocity with static wire (shown in bottom left), the residence time of the particles is longer compared to that of high fluidizing velocity with moving wire (shown in bottom right) [1].

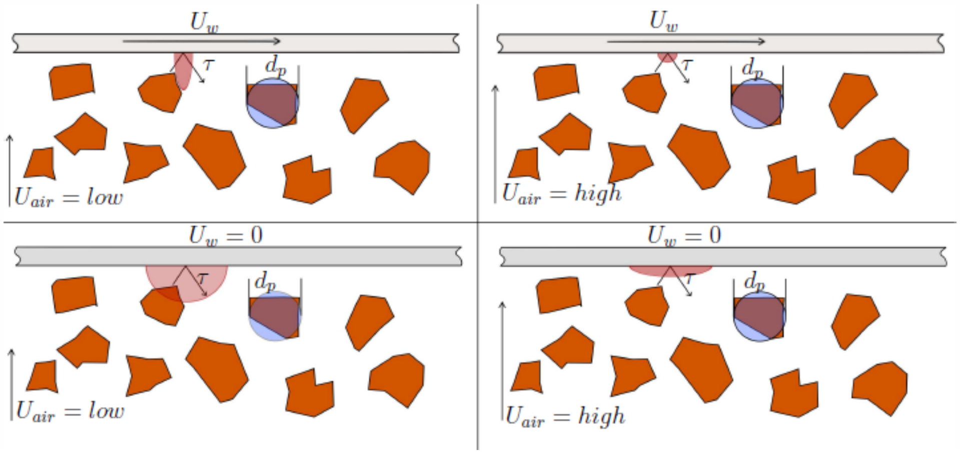

Figure 9: Effects of air velocity and wire speed on particle convection [1].

2.8 Heat Transfer Correlation for Immersed Surfaces

Heat transfer to horizontal cylinders varies with cylinder diameter. Large tubes over 25 mm diameter show a linear relationship between the Nusselt number (Nu) and fluidizing gas flow rate (U_g) [4]. As the fluidizing gas flow increases, Nu increases as a result. In contrast, smaller tubes of 1-10mm diameters show that Nu is nearly constant beyond a fluidizing rate of approximately 2 x U_{mf} [4].

The most commonly used correlation for medium-sized cylinders was developed by Grewal and Saxena [8]. Their developed correlation is shown in Equation 9 below [1]. The main advantage of this correlation was that it was able to predict a wide range of data [8].

$$\mathrm{Nu} = 47(1-\varepsilon)\left[\left(\frac{G\, D_t\, \rho_s}{\rho_g\, \mu_g}\right)\left(\frac{{\mu_g}^2}{d_p^3 \rho_s^2 g}\right)\right]^{0.325} + \left[\frac{\rho_s C_{p,s} D_t^{3/2} g^{1/2}}{k_g}\right]^{0.23} + \mathrm{Pr}^{0.3} \qquad (9)$$

where,

$\mathrm{Nu} = \text{Nusselt Number} \equiv \frac{hD_t}{k_g}$

h = Heat Transfer Coefficient (W/ m^2K)

D_t = Diameter of Immersed Surface (m)

k_g = Thermal Conductivity of the Fluidizing Gas (W/ mK)

G = Mass Flow Rate of the Fluidizing Gas (k_g/s)

$C_{p,s}$ = Specific Heat Capacity of Particles (J/k_gK)

Pr = Prandtl Number of the Fluidizing Gas$\equiv \frac{C_p\, \mu_g}{k_g}$

Bed voidage is defined using Equation 10 [8]:

$$\varepsilon = \frac{1}{2.1}\left[0.4 + \left\{4\left[\frac{\mu_g\, G}{d_p^2\left(\rho_s\left(\rho_s - \rho_g\right)\right)\phi_s^2 g}\right]^{0.43}\right\}^{\frac{1}{3}}\right] \qquad (10)$$

where,

ϕ_s = Sphericity of the Particles

$\phi_s \equiv \frac{\text{Surface Area of a Sphere of Equivalent Volume}}{\text{Surface Area of the Particle}}$

2.9 Small Stationary Cylinders

Even though Grewal and Saxena's (Equation 9) correlation is for boiler tube sized cylinders 25-75 mm diameter, they claimed it is applicable to small diameter cylinder [8]. But when applied to small cylinders in the range 1-8mm of diameters, the shape and magnitude of the curve found using the Grewal and Saxena correlation was not consistent with data. Thus, a new simpler correlation was developed by Friedman et al. [4] which is better suited for small cylinders (i.e. wires) and engineering applications:

$$\mathrm{Nu_{mean}} = \left[1.35\ \mathrm{Ar}^{0.15}\,\frac{\mathrm{d_t}}{\mathrm{d_p}}\right] \tag{11}$$

2.10 Significance of Masoumifard Correlation

A study conducted by Masoumifard et al. [3] on a bed of particles shows that at atmospheric pressure and at low temperature, particle convection is the dominant mode of heat transfer. Later in 2010 another study was conducted by Masoumifard et al. [5] to find the maximum heat transfer coefficient. The study showed that maximum heat transfer is achieved when the contact time (τ) is equal to the duration of time required for the heat to completely diffuse inside the cluster (t_o) [1]. Contact time (τ) is dependent on particle diameter, minimum fluidizing velocity, the ratio of actual and minimum fluidizing velocity and the ratio of particle diameter to immersed surface diameter [5]. Figure 9 illustrates all the above listed parameter and also shows the impact of motion of the immersed surface on contact time (τ).

2.11 Experimental Determination of Heat Transfer Coefficient to a Moving Wire

The heat transfer coefficient cannot be observed and measured directly. It is calculated using measured parameters such as inlet and outlet temperature, fluidized bed temperature, wire speed etc. Figure 10 illustrates the energy balance (excluding radiation) performed on a control volume of moving wire.

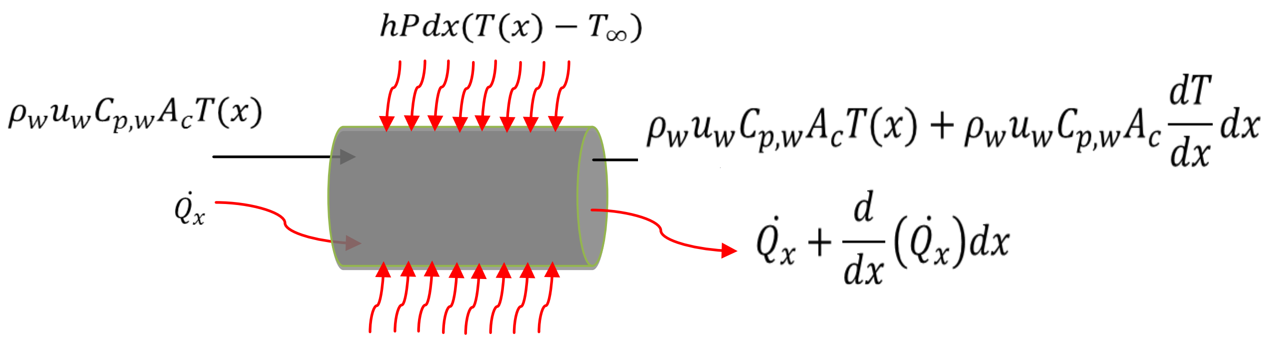

Figure 10: Energy balance on a control volume of moving wire [1].

where,

ρ_w = Density of wire (kg/m^3)

u_w = Wire speed (m/s)

$C_{p,w}$ = Specific heat capacity (J/k_gK)

A_c = Wire cross sectional area (m^2)

P = Wire perimeter (m)

T(x) = Wire temperature at current location (°C)

T_∞ = Bed temperature (°C)

$\dot{Q}_x$ = Conduction heat flux at current location (W/m^2)

h = Average heat transfer coefficient (W/m^2K)

By adding and subtracting the incoming and outgoing conduction, convection and advection terms acting on the control volume and with further manipulation gives the following ordinary differential equation:

$$-k_w A_c \frac{d^2\theta}{dx^2} + \rho_w u_w C_{p,w} A_c \frac{d\theta}{dx} + hP\theta(x) = 0 \qquad (12)$$

This ODE was solved using both analytical and numerical approaches after implementing appropriate boundary conditions. An analytical solution was obtained using Maple software and it is given in Equation 13 below:

$$
\begin{aligned}
\theta(x) = & -[\theta in e^{\frac{1}{2\left(K-\sqrt{K^2+4m^2}\right)}L}\left(-K\sqrt{K^2+4m^2}+K^2+2m^2\right)e^{\frac{1}{2\left(K-\sqrt{K^2+4m^2}\right)}x}]\ / \\
& [e^{\frac{1}{2\left(K-\sqrt{K^2+4m^2}\right)}L}K\sqrt{K^2+4m^2} - e^{\frac{1}{2\left(K-\sqrt{K^2+4m^2}\right)}L}K^2 - 2e^{\frac{1}{2\left(K-\sqrt{K^2+4m^2}\right)}L}m^2 \\
& + e^{\frac{1}{2\left(K-\sqrt{K^2+4m^2}\right)}L}K^2 + 2e^{\frac{1}{2\left(K-\sqrt{K^2+4m^2}\right)}L}m^2 + e^{\frac{1}{2\left(K-\sqrt{K^2+4m^2}\right)}L}K\sqrt{K^2+4m^2}] \\
& + [e^{\frac{1}{2\left(K-\sqrt{K^2+4m^2}\right)}L}\left(K^2+2m^2+K\sqrt{K^2+4m^2}\right)\theta in e^{\frac{1}{2\left(K-\sqrt{K^2+4m^2}\right)}x}]\ / \\
& [e^{\frac{1}{2\left(K-\sqrt{K^2+4m^2}\right)}L}K\sqrt{K^2+4m^2} - e^{\frac{1}{2\left(K-\sqrt{K^2+4m^2}\right)}L}K^2 - 2e^{\frac{1}{2\left(K-\sqrt{K^2+4m^2}\right)}L}m^2\ / \\
& + e^{\frac{1}{2\left(K-\sqrt{K^2+4m^2}\right)}L}K^2 + 2e^{\frac{1}{2\left(K-\sqrt{K^2+4m^2}\right)}L}m^2 + e^{\frac{1}{2\left(K-\sqrt{K^2+4m^2}\right)}L}K\sqrt{K^2+4m^2}]
\end{aligned}
\qquad (13)
$$

where,

θ_{in} = inlet temperature

$$K = \frac{u_w}{\alpha} \qquad (14)$$

$$m^2 = \frac{hP}{kA_c} \qquad (15)$$

But in this approach the parameter ‘h’ could only be solved iteratively which is a tedious process. So a numerical solution to Equation 12 was undertaken starting from an earlier point. The numerical approach is faster and can be obtained easily.

Substituting, $\alpha = \frac{k_w}{\rho_w C_{p,w}}$, $K = \frac{u_w}{\alpha_w}$ and $m^2 = \frac{hP}{k_w A_c}$ into Equation 12 results in the following Equation 16 [1]:

$$\frac{d^2T}{dx^2} - K\frac{dT}{dx} - m^2(T(x) - T_\infty) = 0 \qquad (16)$$

Then performing central differencing on the first term, second order upwinding to the second term of Equation 16 gives [1]:

$$\left(\frac{T_{n+1}-2T_n+T_{n-1}}{\Delta x^2}\right) - K\left(\frac{3T_n-4T_{n-1}+T_{n-2}}{2\Delta x}\right) - m^2(T_n - T_\infty) = 0 \tag{17}$$

Further manipulation results in Equation 18, the solution for this numerical approach in the form of finite difference equation [1]. Comparison between the analytical and numerical solution showed minimal differences between them.

$$T_n = \frac{T_{n+1}+\left(1+\frac{2K}{\Delta x}\right)T_{n-1}-\frac{K}{2\Delta x}T_{n-2}+m^2\Delta x^2 T_\infty}{2+\frac{3K}{2\Delta x}+m^2\Delta x^2} \tag{18}$$

3 Current Work

The main objective of this project was to conduct experiments and analyze the data to develop a simpler correlation using parameters that account for heat transfer to a wire moving in the longitudinal direction.

3.1 Apparatus

The apparatus used in conducting this experiment are:

- **Furnace and Bed:** The pilot scale fluidized bed furnace used was supplied by the ICE Group of Montreal and modified for these experiments [1]. The bed itself consists of three components; furnace plenum, porous hearth tiles and a reducer. The furnace plenum is 1270 mm long × 610 mm wide × 152 mm deep and is covered by three porous hearth tiles with dimensions of 940 mm × 457 mm. A reducer with dimensions of 965 mm × 152 mm was added to allow for higher fluidizing rates. [1]. In this bed two different particle configurations were tested: 1) 65 mm of non-fluidizing coarse aluminum oxide particles (Mean diameter 1000 μm) to distribute air evenly followed by 356 mm of fine particles (Mean diameter 250 μm) 2) 267 mm of non-fluidizing coarse particles (Mean diameter 1000 μm) followed by 154 mm of fine particles (Mean diameter 204 μm) [1]. Figure 11, 13 and 14 illustrates the above components.
- **Air delivery system:** Fluidizing air is delivered by a Spencer multi-stage centrifugal type 3005#2 blower [1]. It is capable of delivering 229.4 m^3/hr of air at 122 kPa [1]. The blower's outlet is connected to a Flow Products venturi flow meter, which is connected to a Dwyer Instruments manometer that measures the differential pressure across the venturi flow meter (shown on Figure 12). This differential pressure is later used to determine air fluidizing velocity.
- **Heating system:** A custom-made 15 KW Chromalox ADHT-015FV heating unit is used for heating the fluidizing air. It is controlled by a panel mounted on a wall. The control panel operates using two parameters with adjustable preset values: desired bed temperature and maximum allowable heater temperature [1].

- **Instrumentation**

    - **Temperature Measurement:** Two Anritsu MW-44K-TC2-ANP contact probes were used to determine the inlet and outlet temperatures of wire [9]. These probes were then connected to a Data Translation DT9828 Data Acquisition Unit (DAQ) for data acquisition [9]. Bed temperature was measured using an immersion type K thermocouple connected to the same DAQ unit.
    - **Data Acquisition:** The hardware used to obtain temperature data for measured parameter is Data Translation DT9828. The DAQ was set to record data at 60Hz and has an accuracy of $\pm$ 0.09 ^{o}C [9]. Data was transferred via USB to the computer and with the aid of QuickDAQ software temperature data was logged and displayed.
    - **Wire Velocity Measurement:** Data for this parameter was obtained using a Shimpo DT-105A Tachometer with $\pm$ 0.006% of reading accuracy or $\pm$ 1 digit [10]. For this experiment the maximum and minimum velocities were measured in m/min but the tachometer is also capable of providing measurements in other units [1].
    - **Flow measurement:** Fluidizing air flow rate was measured using a Flow Products venturi flow meter and a water manometer.

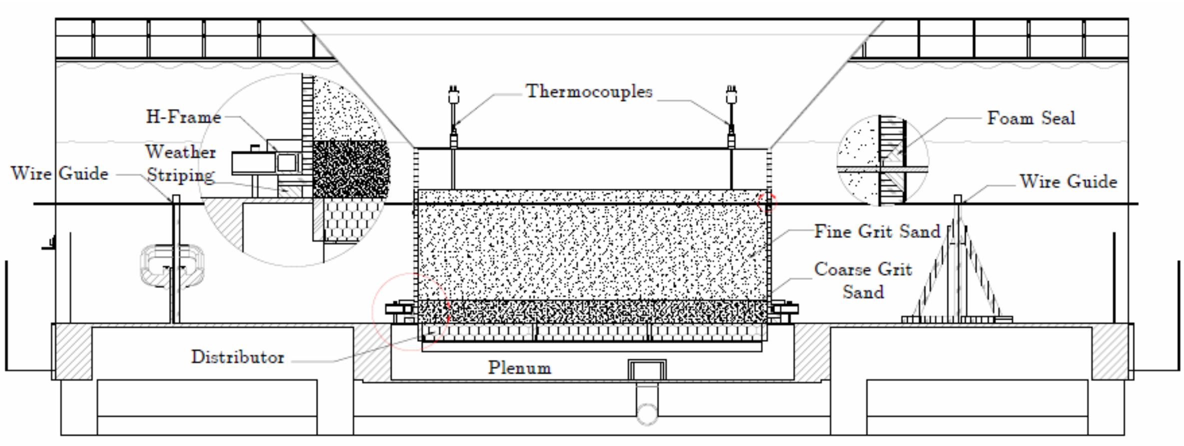

Figure 11: Cross section of fluidized bed [1].

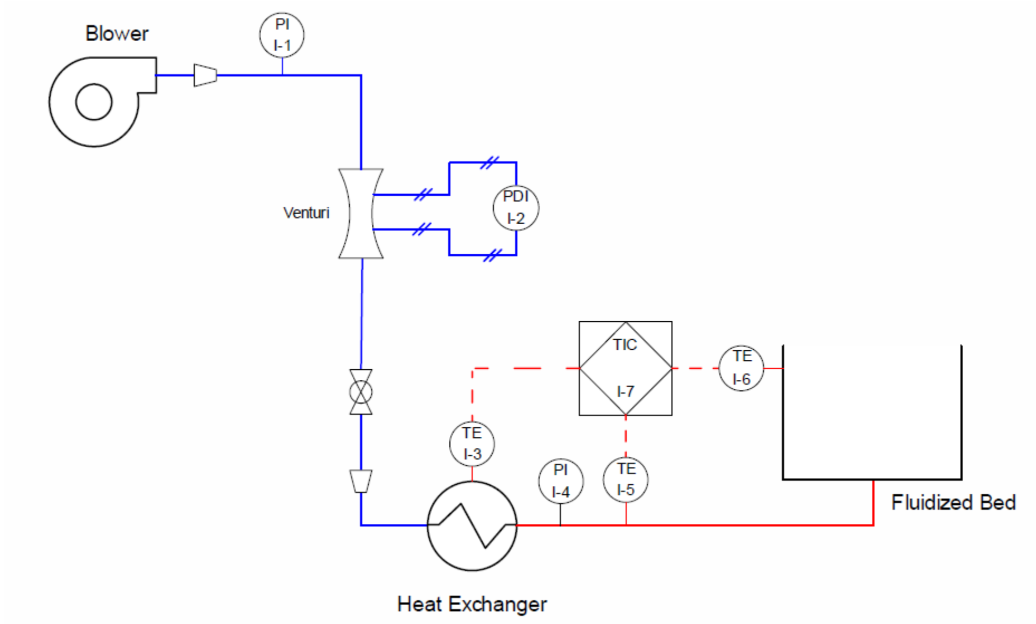

Figure 12: Air delivery and heating system [1].

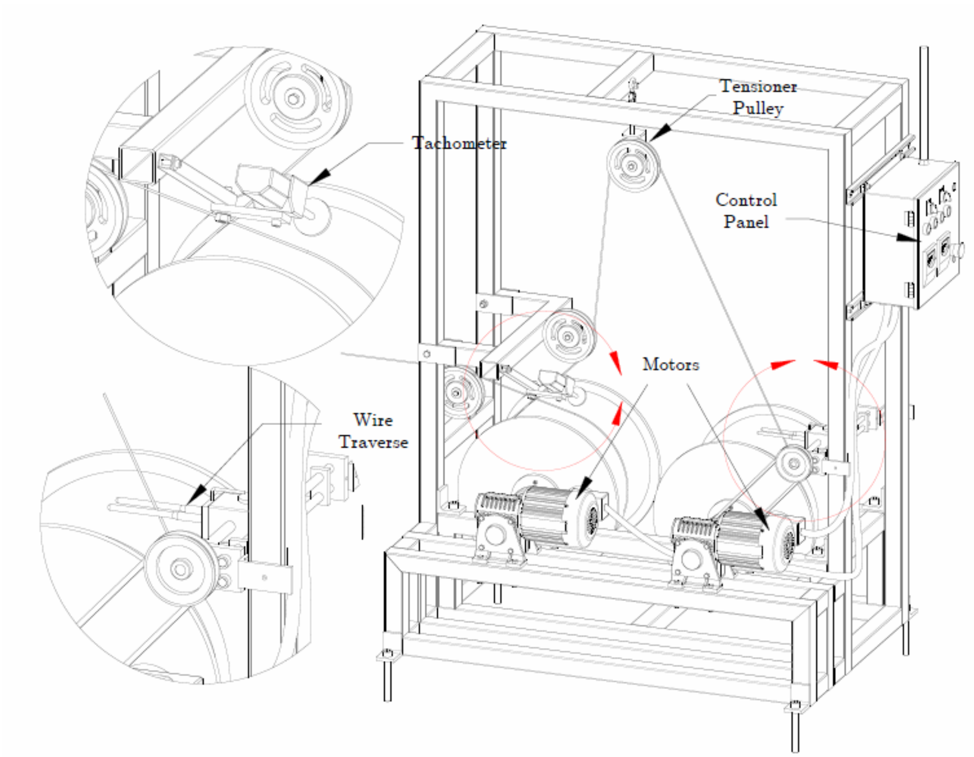

Figure 13: Pulling side of wire movement [1].

Figure 14: Feeding Side of Wire Movement.

3.2 Test Conducted

In this experiment, tests were conducted using two configurations of the fluidized bed and 2.8 mm diameter Aluminum 1188 H18 wire. In the first configuration, 60 grit aluminum oxide particles were used as the fluidized medium and in the second configuration a mix of 70 & 80 grit particles were used. An experimental matrix is shown in Table 1 below, where wire speed was varied in increments of 10 m/min up to 70 m/min.

Table 1: Test conducted at Fluidizing rate of 3 × U_{mf}.

Sand Grit	**Mean Particle Diameter**	**Wire Speed m/min**								
60	**250μm**	**10**	**20**	**30**	**40**	**50**	**55**	**60**	**65**	**70**
70 & 80 Mix	**204 μm**	**10**	**20**	**30**	**40**	**50**	**55**	**60**	**65**	**70**

4 Results and Discussion

4.1 U_{mf} Test

Most industrial wire heat treating fluidizing beds operate between 2.5 to 4 x U_{mf}, where little change of Nusselt number (Nu) is observed. Figure 15 below confirms this finding again. At low, medium and high wire speeds, beyond 3 x U_{mf} less variation in Nusselt number can be observed. However, it is clear that between 1 x U_{mf} and 3 x U_{mf} , there is a strong dependence of Nu on the fluidizing rate U_g. From Figure 15, it can also be concluded that there is a strong dependence between the wire speed and the heat transfer coefficient. This can be attributed to the fact that Nusselt number (Nu) is directly proportional to the heat transfer coefficient as shown on Equation 25.

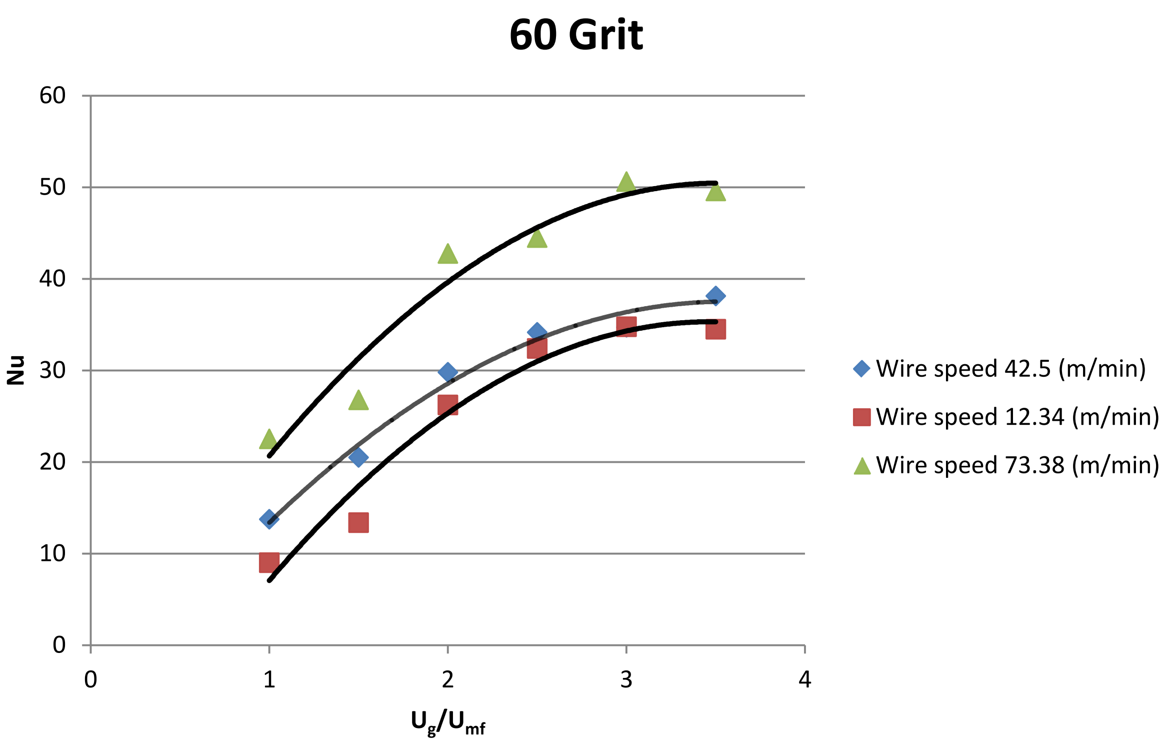

Figure 15: Nusselt numbers at various wire speeds in 60 grit sand.

4.2 60 Grit Tests

Tests were conducted using fluidizing rates from $1 \times U_{mf}$ to $3.5 \times U_{mf}$ at variable wire speed. The findings are illustrated in Figure 16 below. It can be seen that as the fluidizing rate increases the Nusselt number (Nu) also increases. Figure 17 was constructed at $U_g = 3 \times U_{mf}$ with wire speed ranging from 10-75 m/min. It shows two types of error bar where each point is a snapshot of conditions experienced by a moving wire [1]. These error bars are located on the average value of each cluster of points [1]. The horizontal bar represents the uncertainty of wire speed for a specific point measured by a digital tachometer [1]. The vertical bar on the other hand represents the combined experimental error due to instruments, thermocouples, DAQ, tachometer, tolerances of wire diameter etc [1] as discussed in Section 6.

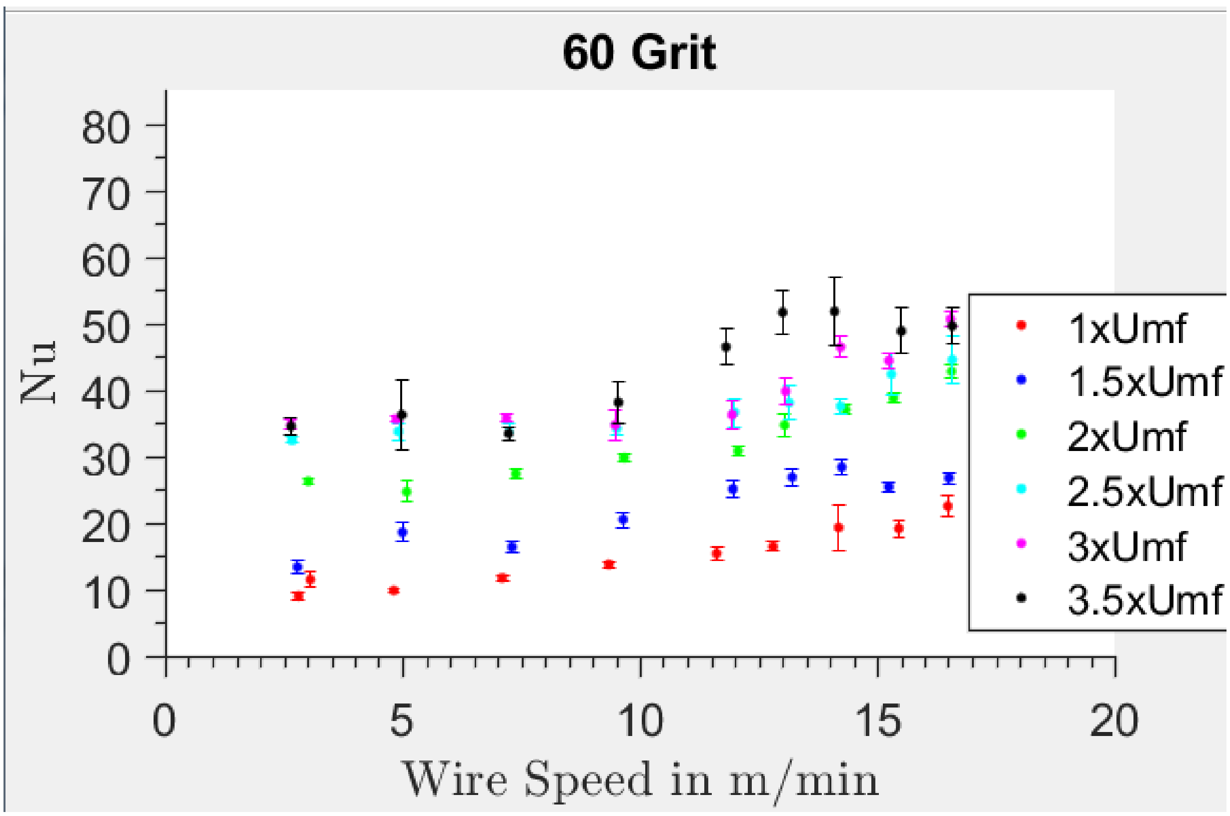

Figure 16: Nusselt numbers at fluidizing rate for 60 grit sand.

4.3 70 - 80 Grits Mix Tests

These tests were initially conducted using 70 grit and 80 grit sand separately. But after the analysis of data a high degree of errors were seen and due to time constraints further experiments were not possible. Therefore, data collected for 70 & 80 grit mix by Tannas [1] in 2015 were used and analyzed.

This 70 & 80 mix grit configuration was tested at fluidizing rate of 3 × U_{mf} with wire speed ranging from 10-75 m/min. Figure 18 below illustrates the findings.

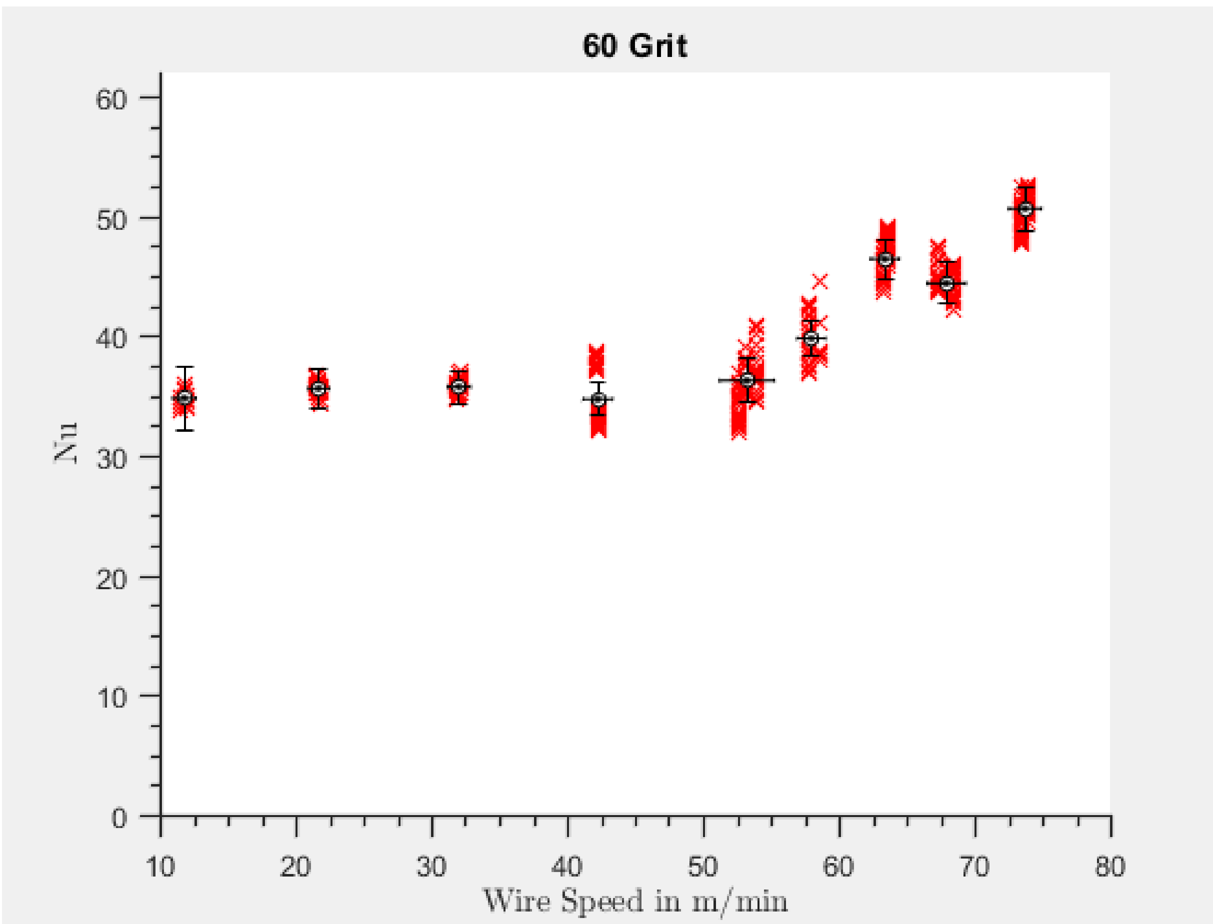

Figure 17: Nusselt numbers at various wire speeds in 60 grit sand (3 x U_{mf}).

4.4 Comparison of 60 and 70 - 80 Grit Mix

From Figure 17 & 18, it can be seen that the 70-80 grit mix particles provide higher Nusselt number compared to 60 grit particles. And it is expected. Both curves show a similar 'U'-like shape. At first Nusselt number increases as the wire speed increases but then it decreases and then again increases. However, the spacing between the points is not consistent throughout the range of wire speed. A larger gap is seen for about 10-50 m/min of wire speed, and then the gap narrows down from 50 m/min upwards.

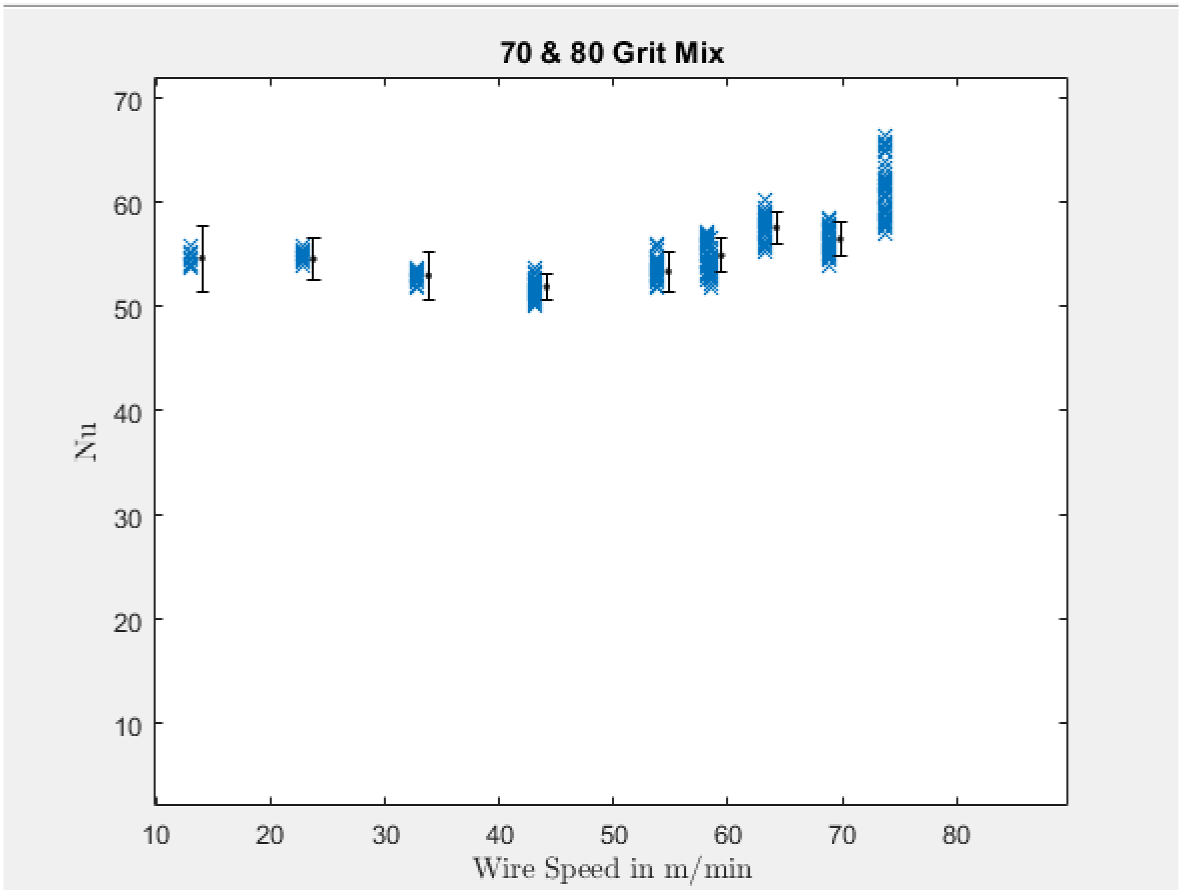

Figure 18: Nusselt numbers at various wire speeds in 70-80 mix grit sand (3 x U_{mf}).

5 New Correlation for Moving Wires

This project was intended to produce a simple correlation suitable for wire heat treating applications. A correlation of the following form was assumed:

$$Nu_{mean,moving}\left(\frac{U_g}{U_{mf}},\frac{U_w}{U_{mf}}\right) = f\left(\frac{U_g}{U_{mf}}\right) + g\left(\frac{U_w}{U_{mf}}\right) \quad (19)$$

From Figures 15 and 16, it is observed that Nusselt number (Nu) is affected by both wire speed and fluidizing rate. Thus, this additive form of correlation includes both wire speed $\left(\frac{U_w}{U_{mf}}\right)$ and fluidizing rate $\left(\frac{U_g}{U_{mf}}\right)$ terms. In this form, the effects of wire speed & fluidizing rate are assumed to be independent of each other. At zero wire speed, the wire speed rate term $g(\frac{U_w}{U_{mf}})$ goes to zero and Nu is only affected by fluidizing rate term $f\left(\frac{U_g}{U_{mf}}\right)$. Figure 18 also shows that at low or near zero wire speed Nu is constant, indicating little influence of wire speed at low speeds.

To determine the fluidization rate and wire speed rate functions, Excel and Excel Solver were utilized. At first, the fluidizing rate function is determined using Figure 15's low wire speed curve. Secondly, the wire speed function is determined using Figure 16. In order to determine the this new correlation given in Equation 20, the experimental data points and the correlation data points were stored in 2 vectors. The correlation data points were generated using equation 20 with the unknown C1, C2, C3 and C4. Next a third vector was created that consisted of the differences of each elements of the previous two vectors. After that the magnitude of the third vector was calculated. To determine the variables C1, C2, C3 and C4, Excel Solver was used. In Excel Solver, the goal was set to reduce the magnitude of the third vector by changing C1, C2, C3 and C4 to change the values of the correlation vector. This resulted in C1, C2, C3 and C4 to be 3.53511, 27.90045, -15.1018, 0.039806 respectively.

Then final form of the correlation became:

$$Nu = \left(C1\left(\frac{U_g}{U_{mf}}\right)^2 + C2\frac{U_g}{U_{mf}} + C3\right) + \left(C4\left(\frac{U_w}{U_{mf}}\right)^2\right) \quad (20)$$

This correlation is valid for $U_g = 1\ U_{mf} - 3.5\ U_{mf}$ and $\frac{U_w}{U_{mf}} \leq 12.34\ \mathrm{m/min}$.

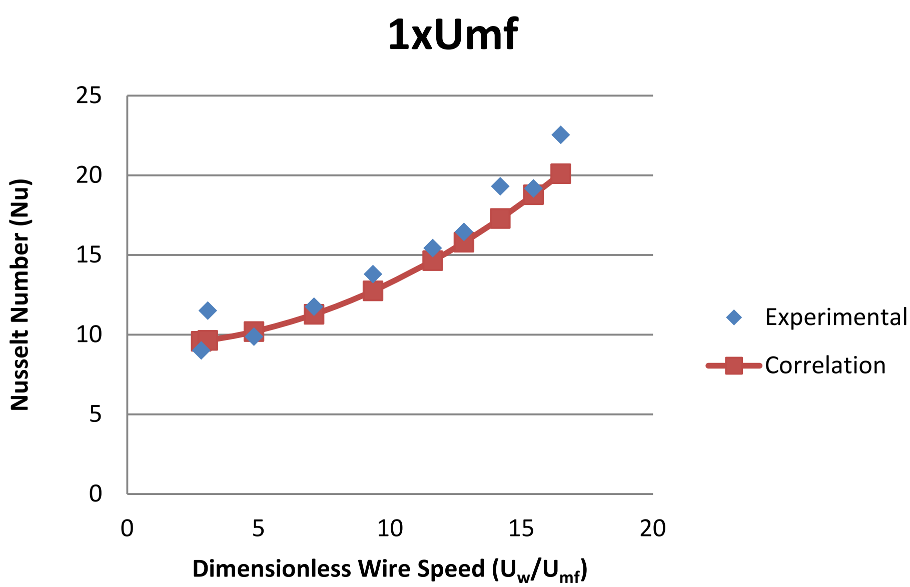

Figure 19: Experimental data vs. correlation for 60 grit sand at 1xU_{mf}.

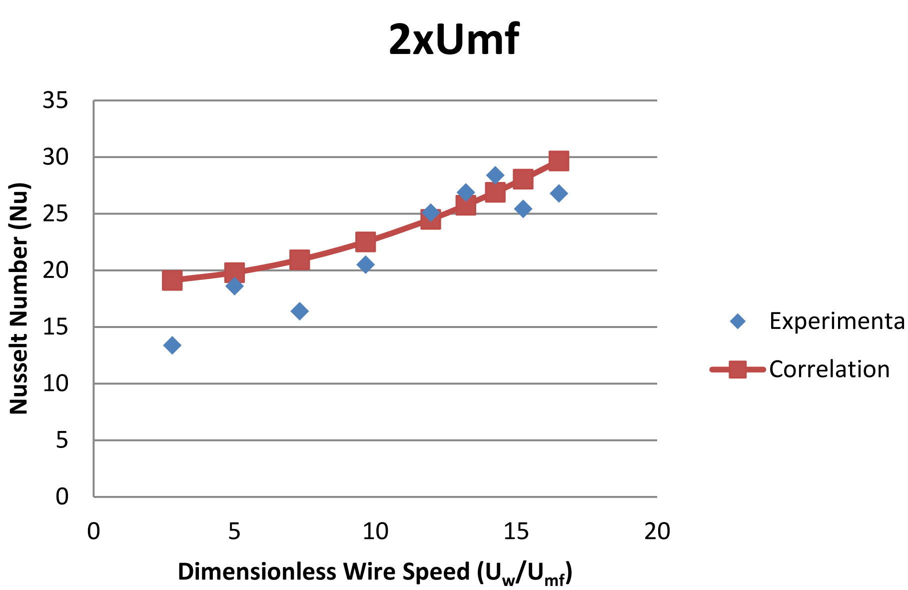

Figure 20: Experimental data vs. correlation for 60 grit sand at 2x U_{mf}.

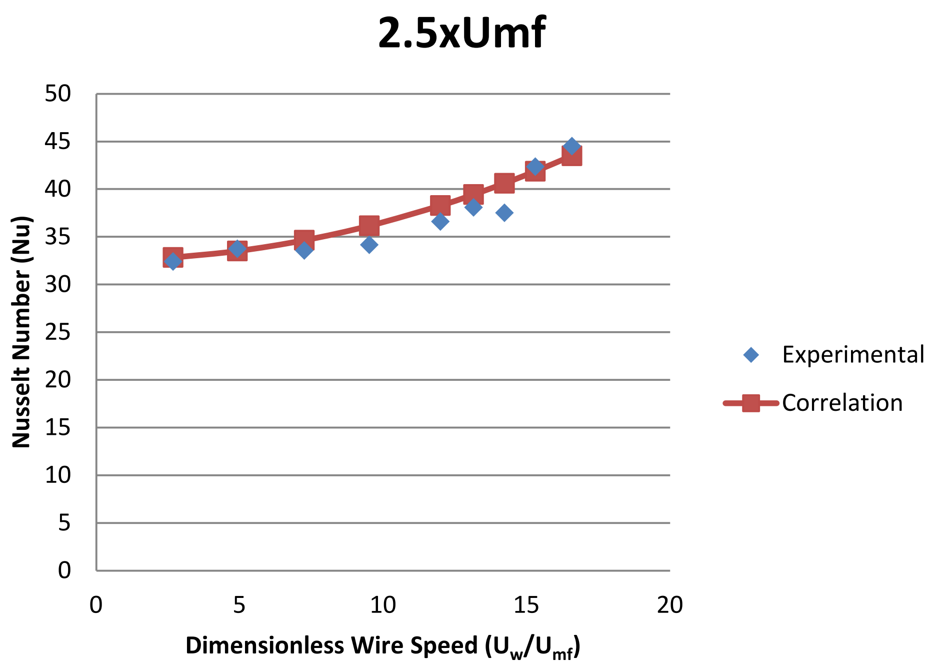

Figure 21: Experimental data vs. correlation for 60 grit sand at 2.5x U_{mf}.

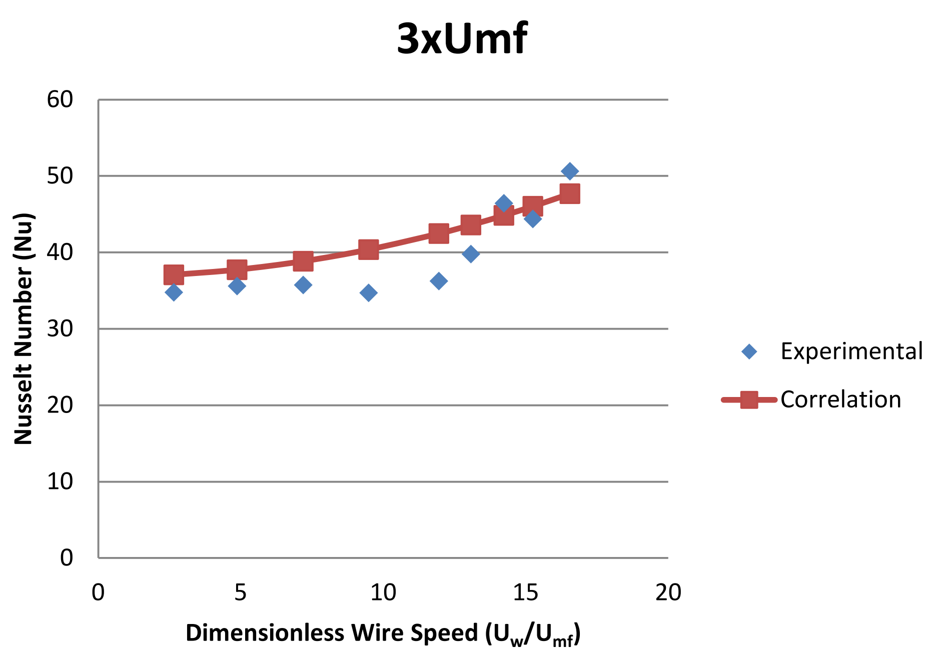

Figure 22: Experimental data vs. correlation for 60 grit sand at 3x U_{mf}.

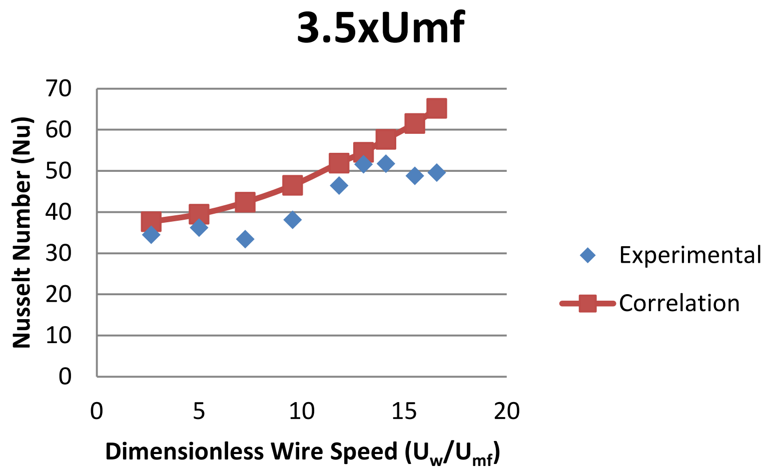

Figure 23: Experimental data vs. correlation for 60 grit sand at 3.5x U_{mf}.

From Figure 19-23, it can be observed that the correlation manages to predict the experimental data quite well for fluidizing rate 1 x U_{mf} to 3.5 x U_{mf}. The increasing parabolic shaped curve fits the 60 grit experimental data approximately within ± 10%. But Equation 20 fails to accurately represent the experimental data for 70 & 80 mix grit sand. From Figure 24 it can be observed that at wire speed below 15 m/min, Equation 20 under-predicts the Nusselt number (Nu). Therefore, more experimental data and more terms are required to accurately represent different grit sizes.

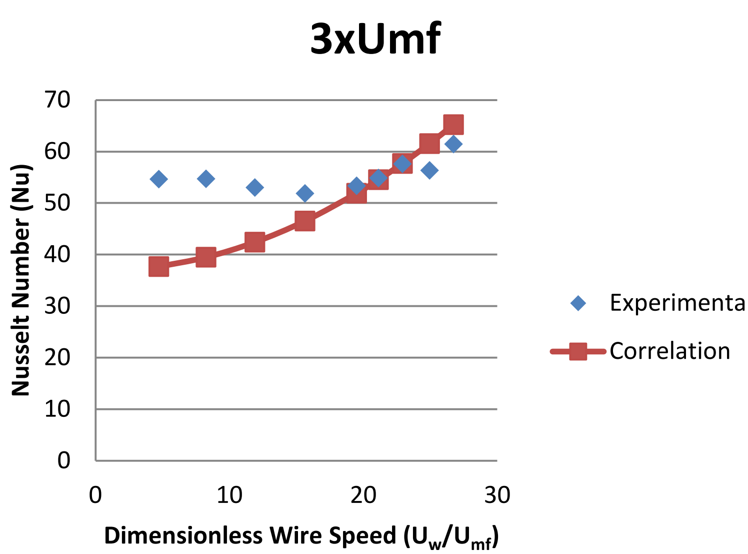

Figure 24: Experimental data vs. correlation for 70 and 80 mix grit sand at 3xU_{mf}

6 Error Assessment

An error assessment was conducted to identify uncertainties that affect the accuracy of the heat transfer coefficient calculations.

- **Air flow Uncertainties**

A Venturi flow meter is used to measure the air flow rate going into the fluidized bed. The current flow rate is measured using Equation 21 [1]:

$$\frac{G}{G_{ref}} = \sqrt{\frac{\Delta p}{\Delta p_{ref}}} \quad (21)$$

Where, G= Measured air flow rate (m^3/hr)

G_{ref} = Reference flow rate (254 m^3/hr)

Δp = Measured pressure drop (mm of water)

Δp_{ref} = Reference pressure drop (378.46 mm of water)

The error in flow rate is calculated using Equation 22 [11]:

$$\frac{\Delta y}{y} = n\frac{\Delta x}{x} \quad (22)$$

Where, y = G, measured air flow rate

Δy = Error in air flow rate

$x = \frac{\text{Measured pressured drop}}{\text{Reference pressure drop}}$

Δx = Error in pressure drop (measured precision of Dwyer Instruments manometer is $\pm$ 0.1 inch or $\pm$ 2.54 mm [1])

The pressure drop and flow rate in this experiment varied from 30.48 (1.2" water Δp) - 101.6 mm (4") and 72.2 m^3/hr - 132 m^3/hr consecutively [1]. And as the bubbling in the fluidizing bed increased, the measured pressure drop fluctuated due to bubble pressure pulses. The range of error calculated using Equation 22 is found to be $\pm$ 1.95 m^3/hr (for lower range of flow rates) and $\pm$ 1.65 m^3/hr (1.25%) (for higher range of flow rates) [1].

The uncertainty change in pressure drop becomes smaller with increasing flow rates.

- **Heat transfer Uncertainties**

In this experiment, the heat transfer was calculated using an iterative method. The effect of convection was much larger than axial conduction, so axial conduction was ignored [1].

The heat transfer coefficient (h) was calculated using Equation 23 [1]:

$$h = -\frac{\rho_w u_w C_{p,w} D_t}{4L} \times \ln\left(\frac{T_{out} - T_\infty}{T_{in} - T_\infty}\right) \tag{23}$$

The heat transfer coefficient error is calculated using Equation 24 [1]:

$$\Delta h = h \times \left\{ \left[\frac{(\frac{\Delta\rho_w}{\rho_w})^2 + (\frac{\Delta u_w}{u_w})^2 + (\frac{\Delta C_{p,w}}{C_{p,w}})^2 + (\frac{\Delta D_t}{D_t})^2 + (\frac{\Delta L}{L})^2}{\left(-\frac{\rho_w u_w C_{p,w} D_t}{4L}\right)^2} \right] + \frac{\frac{{T_{out}}^2 + {T_\infty}^2}{(T_{out} - T_\infty)^2} + \frac{{T_{in}}^2 + {T_\infty}^2}{(T_{in} - T_\infty)^2}}{(\ln(\frac{T_{out} - T_\infty}{T_{in} - T_\infty}))^2} \right\}^{1/2} \tag{24}$$

The maximum error range in h was found to be between $\pm$ 25 W/m^{2}K (5.3%) at 475 W/m^{2}K and $\pm$ 17 W/m^{2}K (2.7%) at 630 W/m^{2}K [1].

The Nusselt number is defined as the ratio of convective to conductive heat transfer and shown in Equation 25 [1]:

$$Nu = \frac{hD_t}{k_g} \tag{25}$$

where, h = heat transfer coefficient

D_t = Wire diameter

k_g = Thermal conductivity of gas (air)

Nusselt number error is calculated using Equation 26 [1]:

$$\Delta Nu = Nu \times \left\{ \left(\frac{\Delta h}{h}\right)^2 + \left(\frac{\Delta D_t}{D_t}\right)^2 + \left(\frac{\Delta kg}{kg}\right)^2 \right\}^{1/2} \tag{26}$$

The error in Nusselt number was found to range between maximum of $\pm$ 2.6 at 47 (5.53%) and $\pm$ 2.1 at 61.5 (3.41%) [1].

- **Wire Speed Uncertainties**

  Wire speed was measured using a DT-105A tachometer. It is incapable of any data logging but can display the maximum and minimum value for each run [1]. On average, two runs per each set speed were taken. On each run, mean wire speed (between the maximum & minimum) was taken to be the actual wire speed. Then the error was calculated by taking the difference between the mean and the maximum & the minimum value [1]. Additional error in wire speed measurement came from tachometer itself, which has an accuracy of $\pm$ 0.39 m/min [1].

- **Other Uncertainties**

  In addition to the above uncertainties, some other factors can impact the heat transfer determination. They are: chaotic nature of bubbles as well as relative humidity [1]. From Figure 17 & 18 wide scatter in heat transfer coefficient is observed at higher speeds. Inside the fluidized bed at high speed, the wires element’s residence time decreases when residence time is short compared to the time scale of bubbles (approximately 0.55), a fair bit of scatter is expected as the wire is not immersed long enough for the chaotic nature of bubbles to "average out" [1]. And since the diameter of the wire which passes though the middle of the bed is only 1.84% of the width of the bed, exposure to bubbling can result in very high or very low heat transfer [1]. Humidity is another phenomenon that can affect the result. At higher humidity, inter-particle adhesion increases [1]. This causes the sand particles to stick with each other, making it harder for particles to fluidize [1].

7 Conclusion

The main objective of this project was to conduct more experiments and to obtain more data for analysis. Experiments were conducted using 60 grit sand and 70 and 80 grit mix sand on the pilot scale wire moving system developed by Tannas [1]. After the data analysis a new simpler correlation was developed by taking both wire speed & fluidizing rate term into consideration:

$$\mathrm{Nu} = \left(-3.53511\left(\frac{\mathrm{U_g}}{\mathrm{U_{mf}}}\right)^2 + 27.90045\,\frac{\mathrm{U_g}}{\mathrm{U_{mf}}} - 15.1018\right) + \left(0.0039806\left(\frac{\mathrm{U_w}}{\mathrm{U_{mf}}}\right)^2\right)$$

$$\text{valid for } \mathrm{U_g} = 1\ \mathrm{U_{mf}} - 3.5\ \mathrm{U_{mf}}\ \&\ \frac{\mathrm{U_w}}{\mathrm{U_{mf}}} \leq 12.34\ \mathrm{m/min}$$

This correlation is found to predicts the experimental data for 60 grit sand within $\pm$ 10%.

8 References

1. Tannas, Antonio. *Heat Transfer to a Moving Wire Immersed in a Gas Fluidized Bed Furnace*. Thesis. Toronto, Ontario, Canada, Ryerson University, 2015.
2. Geldart, D. Gas fluidization technology. John Wiley and Sons Inc., New York, NY, 1986.
3. Masoumifard, N., Mostoufi, N., Hamidi, A.A., and Sotudeh-Gharebagh, R. Investigation of heat transfer between a horizontal tube and gas–solid fluidized bed. *International Journal of Heat and Fluid Flow*, 29(5):1504–1511, 2008.
4. Friedman, J., Koundakjian, P., Naylor, D., and Rosero, D. Heat transfer to small horizontal cylinders immersed in a fluidized bed. *Journal of heat transfer*, 128(10):984-989, 2006.
5. Masoumifard, N., Mostoufi, N., & Sotudeh-Gharebagh, R.. Prediction of the Maximum Heat Transfer Coefficient Between a Horizontal Tube and Gas–Solid Fluidized Beds. *Heat Transfer Engineering*, 870-879, 2010.
6. Desai, Chetan Jitendra. *Heat transfer to a stationary and moving sphere immersed in a fluidized bed*. Retrospective Theses and Dissertations. Paper 8926. United States, Iowa State University,1989.
7. Ommen, J. Ruud van, Ellis, Naoko. "Fluidization". JMBC/OSPT course Particle Technology 2010.
8. Grewal, N., and Saxena, S. Heat transfer between a horizontal tube and a gas-solid fluidized bed. *International Journal of Heat and Mass Transfer, 23*(11), 1505-1519, 1980.
9. Data Translation. DT9282 User's Manual, 2014b
10. Data Translation. DT9282 Data Sheet, 2014a
11. A Summary of Error Propagation - Harvard University. From http://ipl.physics.harvard.edu/wp-uploads/2013/03/PS3_Error_Propagation_sp13.pdf
12. Geldart, D. Types of gas fluidization. *Power technology*, 7(5):285-292,1973.
13. Penny, C., Naylor, D., & Friedman, J. Heat transfer to small cylinders immersed in a packed bed. *International Journal of Heat and Mass Transfer, 53*(23-24), 5183-5189, 2010